AIMS Mathematics, 9(4): 8661–8688.
DOI: 10.3934/math.2024420
Received: 01 December 2023
Revised: 18 February 2024
Accepted: 23 February 2024
Published: 29 February 2024

http://www.aimspress.com/journal/Math

Research article

An efficient numerical technique for investigating the generalized Rosenau–KDV–RLW equation by using the Fourier spectral method

Shumoua F. Alrzqi[1], **Fatimah A. Alrawajeh**[1] **and Hany N. Hassan**[2,*]

[1] Department of Mathematics, College of Science, Imam Abdulrahman Bin Faisal University, P.O. Box 1982, Dammam, Saudi Arabia

[2] Department of Basic Sciences, Deanship of Preparatory Year and Supporting Studies, Imam Abdulrahman Bin Faisal University, P. O. Box 1982, Dammam, Saudi Arabia

* **Correspondence:** Email: Hngomaa@iau.edu.sa.

Abstract: In this article, the generalized Rosenau-Korteweg-de Vries-regularized long wave (GR–KDV–RLW) equation was numerically studied by employing the Fourier spectral collection method to discretize the space variable, while the central finite difference method was utilized for the time dependency. The efficiency, accuracy, and simplicity of the employed methodology were tested by solving eight different cases involving four examples of the single solitary wave with different parameter values, interactions between two solitary waves, interactions between three solitary waves, and evolution of solitons with Gaussian and undular bore initial conditions. The error norms were evaluated for the motion of the single solitary wave. The conservation properties of the GR–KDV–RLW equation were studied by computing the momentum and energy. Additionally, the numerical results were compared with the previous studies in the literature.

Keywords: GR–KDV–RLW equation; Fourier spectral method; fast Fourier transform; finite difference; solitary waves
Mathematics Subject Classification: 35C08, 65M06, 65T50

1. Introduction

Solving nonlinear partial differential equations (NLPDEs) has become a useful tool for delineating numerous physical problems that arise in many fields of mathematics and science, which includes describing various types of wave behavior observed in the natural world, with applications such as fluid mechanics to solid-state physics, plasma physics, nonlinear optics, etc. This made the nonlinear wave phenomena a major focus of scientific research in recent decades. Many researchers have diligently developed a wide range of powerful techniques to uncover solutions for NLPDEs both

analytically and numerically. For instance, the Korteweg-de Vries (KdV) equation is frequently employed to model small-amplitude, and long waves on various surfaces, including shallow water, ion sound, and longitudinal astigmatic waves. The regularized long-wave (RLW) equation stands as a versatile model encompassing a wide range of physical phenomena. It not only characterizes shallow water waves, but also captures the intricate dynamics of nonlinear dispersive waves, ion-acoustic plasma waves, and magnetohydrodynamic plasma waves. To date, numerous numerical methods have been utilized to simulate solitary waves in the context of the Rosenau-Korteweg-de Vries (R-KdV) and Rosenau-KdV-RLW equations. However, there exists a limited number of numerical schemes specifically designed for the accurate simulation of shock waves in these equations. In this article, we aim to comprehensively address this research gap. To begin, the KdV equation stands as the quintessential model for investigating weakly nonlinear long waves that emerge in physical systems. For instance, it serves as a valuable descriptor for phenomena like shallow water surface waves with long wavelengths and small amplitudes, as well as internal waves within shallow density-stratified fluids. Beyond these examples, the KdV equation finds utility in a multitude of other applications, encompassing plasma waves, Rossby waves, and magma flow [1]. Korteweg and de Vries suggested the KdV equation as [2, 3] :

$$u_t + auu_x + bu_{xxx} = 0. \tag{1.1}$$

Within this equation, a real-valued function is denoted as u, alongside two real constants, a and b. This equation forms the fundamental basis for exploring and understanding waves of this particular nature [1, 4]. To depict the behavior of dense discrete systems, Philip Rosenau introduced what we now refer to as the Rosenau equation in 1988, which takes the following form [5, 6]:

$$u_t + u_x + cu_{xxxxt} + d(u^2)_x = 0. \tag{1.2}$$

In a deeper exploration of nonlinear waves, Zuo [7] modified the Rosenau equation (1.2) by adding the viscous term u_{xxx}, leading to the what is now known as the R-KdV equation:

$$u_t + au_x + bu_{xxx} + cu_{xxxxt} + d(u^2)_x = 0. \tag{1.3}$$

The authors effectively obtained solitons and periodic wave solutions for the model by merging the KdV equation and the Rosenau equation, which was achieved by using both the sine-cosine and tanh methods in [4, 7]. In [8], the conservative linear difference scheme was created for the R-KdV equation. The authors introduced the modified variational iteration algorithm-II (MVIA-II) to obtain numerical solutions of different types of fifth-order KdV equations [9]. In [10], the authors focus on deriving solitary wave solutions for the generalized Rosenau-KdV equation using the sech-ansatz method. Through the examination of various test problems, these methods showcase both efficiency and reliability in their application. The inclusion of the term $-u_{xxt}$ in Eq (1.3), when $b = 0$, describes an additional characteristic of nonlinear waves, leading to what is commonly referred to as the Rosenau–RLW equation:

$$u_t + au_x + cu_{xxxxt} + d(u^2)_x - eu_{xxt} = 0. \tag{1.4}$$

This equation represents a significant model in nonlinear wave studies. Furthermore, its extended form is known as the generalized Rosenau–RLW equation:

$$u_t + au_x + cu_{xxxxt} + d(u^p)_x - eu_{xxt} = 0. \tag{1.5}$$

The generalized Rosenau–RLW equation presents an expanded framework for understanding complex nonlinear wave behaviors, incorporating the effect of U over time within the wave equation's dynamics. This equation holds significance in the realm of nonlinear wave theory, providing a foundation for studying the behaviors and characteristics of waves within different physical systems. In this article, the generalized Rosenau–KDV–RLW (GR–KDV–RLW) equation will be considered, which combines terms from the generalized Rosenau KDV and generalized Rosenau–RLW equations. The provided equation can be represented as follows:

$$u_t + au_x + b^{KdV}u_{xxx} + cu_{xxxxt} + d(u^p)_x - e^{RLW}u_{xxt} = 0. \tag{1.6}$$

It's important to note that in this context, $p \geq 2, d > 0, a, b^{KdV}, c$, and e^{RLW} are real constants [11,12]. We impose specific physical boundary conditions, requiring that $u \to 0$ as $x \to \pm\infty$. The variables x and t indicate differentiation with respect to space and time, respectively. To apply our numerical method effectively, we confine our solution to the interval defined by $a \leq x \leq b$. The shallow water wave equation can be represented numerically using the dependent variable $u(x,t)$, denoting the wave profile concerning spatial position (x) and time (t). The equation includes coefficients such as a for drift effect, b for third-order dispersion, c for higher-order dispersion, and d for nonlinear effects. e represents the coefficient associated with the term u_{xtt}, contributing to the evolution of shallow water waves. Boundary conditions will be selected from a set of homogeneous conditions for further analysis.

$$\begin{aligned} &u(a,t) = 0, \quad u(b,t) = 0, \\ &u_x(a,t) = 0, \quad u_x(b,t) = 0, \quad t > 0. \end{aligned} \tag{1.7}$$

Furthermore, the initial condition is defined as :

$$u(x,0) = f(x), \quad a \leq x \leq b. \tag{1.8}$$

Given the known value of $f(x)$, Eq (1.6) combines the general Rosenau-KdV and general Rosenau-RLW equation. By setting b^{KdV} to zero in Eq (1.6), the resulting equation represents the general Rosenau-RLW as follows:

$$u_t + au_x + cu_{xxxxt} + d(u^p)_x - e^{RLW}u_{xxt} = 0, \quad p \geq 2. \tag{1.9}$$

In the Eq (1.9), for $p = 2$, it represents the usual Rosenau-RLW equation, and for $p = 3$, it denotes the modified Rosenau-RLW equation. Moreover, in Eq (1.6) for $p \geq 4$, it signifies the general Rosenau-RLW equation. The Rosenau–KDV–RLW equation has prompted the development of various numerical schemes. However, the generalized form of the Rosenau–KDV–RLW equation has received comparatively less focus owing to its height nonlinearity. Numerous numerical techniques have been put forth to address the Rosenau-KdV equation, including methods where [13] introduced an innovative approach merging the Haar wavelet collocation method, a nonstandard finite difference scheme, and quasilinearization to calculate numerical solutions for the given equation effectively. [14] proposes semi-discrete and fully-discrete B-spline Galerkin approximations. The approach involves applying a proper orthogonal decomposition (POD) method to a Galerkin finite element (GFE)

formulation. [15] presents a third-order weighted essentially non-oscillatory (WENO) method combined with a four stage third-order L-stable SSP implicit-explicit Runge-Kutta method (Third-order SSP EXRK method and third-order DIRK method) for spatial and temporal discretization. [16] introduces two highly effective numerical schemes that rely on a combination of the B-spline finite element method and time-splitting techniques. [17] proposes a meshless algorithm using radial basis function and finite-difference methods to approximate the solution of the equation. In [18], a collocation technique based on quintic B-spline basis functions is proposed and they apply the Runge–Kutta method of four stages and third-order (SSP-RK43) to solve the resulting system of equations. [19] presents a collocation finite element method based on septic B-splines, which provides better numerical solutions compared to previous methods. [20] proposes a two-level implicit fully discrete scheme with third-order accuracy in space and second-order accuracy in time. In both [21, 22], numerical methods are introduced with a common foundation in B-spline collocation finite element techniques, applied to solve specific equations. [23] proposes a three-level linear implicit conservative scheme that is second-order convergent and unconditionally stable. The spectral collocation method has been applied in previous literature as a computational technique, such as shown through [24–33]. In this article, the GR–KDV–RLW equation will numerically analyze by employing the fast Fourier transform (FFT) technique combined with the central difference method. The GR–KDV–RLW equation will be addressed and solved across eight different cases, which encompasses the behavior of single solitary waves, interactions among two and three solitary waves, and the evolution of solitons with Gaussian and undular bore initial conditions.

2. Materials and methods

2.1. Preliminary

In [23], the authors present the following results to ensure the Eqs (1.6)–(1.8) when $c = 1$ are well-posed and satisfy conservation laws, the solution, and its derivatives. When considering the L_2 norm, the solution and its derivatives are bounded up to the second order. Also, when considering the L_∞ norm, both the solution and its first-order derivative remain confined [13]. Equivalent results can be easily obtained for other values of c.

Definition 2.1. Let $\Omega = [a, b]$ and $u^{(q)}$ represent the q-th order derivative. The Sobolev spaces $H^2(\Omega)$ and $H_0^2(\Omega)$ are defined as follows:

$$H^2(\Omega) = \left\{ u : \int_\Omega \left(u^{(q)}\right)^2 dx < \infty,\ q = 0, 1, 2 \right\}, \tag{2.1}$$

$$H_0^2(\Omega) = \left\{ u : u \in H^2(\Omega), \frac{\partial^i u}{\partial x^i} = 0 \text{ on } \partial\Omega \quad i = 0, 1, 2 \right\}. \tag{2.2}$$

Lemma 2.1. *Suppose $u_0 \in H_0^2[a, b]$, then the solution of Eqs* (1.6)–(1.8) *satisfies*

$$I_M(t) = \int_a^b u(x, t)dx = \int_a^b u(x, 0)dx = \int_a^b u_0 dx = I_M(0).$$

Theorem 2.1. *Suppose $u_0 \in H_0^2[a,b]$, then the solution of Eqs* (1.6)–(1.8) *satisfies*

$$I_E(t) = \int_a^b \left[u^2(x,t) + eu_x^2(x,t) + cu_{xx}^2(x,t)\right] dx = \|u\|_{L_2}^2 + e\,\|u_x\|_{L_2}^2 + c\,\|u_{xx}\|_{L_2}^2 = I_E(0), e \geq 0.$$

Theorem 2.2. *Suppose $u_0 \in H_0^2[a,b]$, then the solution of Eqs* (1.6)–(1.8)*, satisfies $\|u\|_{L_2} \leq C, \|u_x\|_{L_2} \leq C, \|u_{xx}\|_{L_2} \leq C$, and, hence $\|u\|_{L_\infty} \leq C$ and $\|u_x\|_{L_\infty} \leq C$.*

Theorem 2.3. *Suppose $u_0 \in H_0^2[a,b]$, then the problem defined by Eqs* (1.6)–(1.8) *is well-posed.*

2.2. Analysis of the numerical scheme

In the realm of numerical methods, a sophisticated method is developed specifically for tackling the periodic initial value problem that's encountered. This problem is presented with a scenario wherein a function denoted as u is predefined as a prescribed function of x at the initial time point $t = 0$, and, subsequently, the solution exhibits periodic behavior concerning the variable x while being constrained within a fundamental interval defined by $a \leqslant x \leqslant b$. The Eq (1.6) can be written as:

$$w_t = -au_x - bu_{xxx} - d(u^p)_x. \tag{2.3}$$

Simplification of Eq (2.3) yields:

$$w_t = -au_x - bu_{xxx} - (p)du^{p-1}(u)_x, \tag{2.4}$$

where

$$w = u + cu_{xxxx} - eu_{xx}. \tag{2.5}$$

For a clearer presentation, the spatial period $[a,b]$ will be normalized to $[0,2\pi]$ via the transformation $x \to \frac{2\pi(x-a)}{L}$, where $L = b - a$. The normalization process extends to the Fourier space in relation to x and its derivatives or other operators related to x. The FFT efficiently performs this process, then, by employing the inverse Fourier transform, expressed as $\frac{\partial^n u}{\partial x^n} = F^{-1}(ik)^n F(u)$ for $n = 1, 2, \ldots$, we proceed to discretize the resulting equations. For any positive integer N, we consider grid points $x_j = j\Delta x = \frac{2\pi j}{N}$, where $j = 0, 1, \ldots, N-1$. The solution $u(x,t)$ is subsequently transformed into discrete Fourier space as follows:

$$\hat{u}(k,t) = F(u) = \frac{1}{N}\sum_{j=0}^{N-1} u\left(x_j,t\right)e^{-ikx_j}, \quad -\frac{N}{2} \leqslant k \leqslant \frac{N}{2} - 1. \tag{2.6}$$

The inverse formula is

$$u\left(x_j,t\right) = F^{-1}(\hat{u}) = \sum_{k=-N/2}^{N/2-1} \hat{u}(k,t)e^{ikx_j}, \quad 0 \leqslant j \leqslant N-1. \tag{2.7}$$

To simplify, we use the Fourier transform on both sides of Eqs (2.4) and (2.5) to represent them in Fourier space:

$$\hat{w}(k,t) = -aik\hat{u}(k,t) - b(ik)^3\hat{u}(k,t) - pd(ik)\hat{u}^{p-1}(\hat{u})_x(k,t), \tag{2.8}$$

$$\hat{w}(k,t) = \hat{u}(k,t) + c(ik)^4\hat{u}(k,t) - e(ik)^2\hat{u}(k,t). \tag{2.9}$$

Now, all the mathematical operations mentioned earlier will be applied to Eqs (2.4) and (2.5), ultimately reducing them to the following equation:

$$w(x_j,t) = u(x_j,t) + c(2\pi/L)^4F^{-1}\{k^4F(u)\} - e(2\pi/L)^2F^{-1}\{-k^2F(u)\}, \tag{2.10}$$

$$\frac{\partial w(x_j,t)}{\partial t} = -a(2\pi/L)F^{-1}\{ikF(u)\} - b(2\pi/L)^3F^{-1}\{-ik^3F(u)\} - d(2\pi/L)^p u^p(x_j,t)F^{-1}\{ikF(u)\}. \tag{2.11}$$

Let $\boldsymbol{u} = [u(x_0,t), u(x_1,t), \ldots, u(x_{N-1},t)]^T$.

The ordinary differential equation (2.11) can be expressed in vector form as:

$$\boldsymbol{w_t} = g(\boldsymbol{u}). \tag{2.12}$$

The function $g(\boldsymbol{u})$ is defined as the righthand side of the equation, which can be solved using various methods from first-order differential equations. Specifically, in this article, the central finite differences method will be employed. Regarding its convergence and stability, its efficacy is discussed in [34–36]. By utilizing the inverse Fourier transform as defined in Eq (2.7), the next step is to simplify Eq (2.8), resulting in the reduction of the derived equation. Introduce the central difference method as follows:

$$w_t = \frac{w(x,t+\Delta t) - w(x,t-\Delta t)}{2\Delta t} = \frac{w^{n+1} - w^{n-1}}{2\Delta t}. \tag{2.13}$$

By applying the scheme to handle the resulting ordinary differential equation in the time domain and, by employing it to advance in time, we achieve the following result:

$$w(x,t+\Delta t) = w(x,t-\Delta t) + 2\Delta t g(u(x,t)). \tag{2.14}$$

Finally, in our pursuit of a solution, we employ the inverse Fourier transform to approximate our result. The central difference method necessitates the provision of two distinct initial values, which is fundamental to its operation. To start this process, we define the first of these two levels and start with $u(x,0)$ to reach $w(x,0)$, then

$$w(x,n\Delta t) = F^{-1}(1 + ck^4(2\pi/L)^4 - ek^2(2\pi/L)^2)F(u(x,n\Delta t)), \tag{2.15}$$

$$w(x,0) = F^{-1}(1 + ck^4(2\pi/L)^4 - ek^2(2\pi/L)^2)F(u(x,0)). \tag{2.16}$$

To compute the second level of the initial solution denoted as $w(x,\Delta t)$, we utilize a higher-order one-step method, specifically, the fourth-order Runge-Kutta method (RK4).

$$
\begin{aligned}
K_1 &= F(u(x,0),0),\\
K_2 &= F(u(x,0)+\frac{1}{2}\Delta t K_1,\frac{1}{2}\Delta t),\\
K_3 &= F(u(x,0)+\frac{1}{2}\Delta t K_2,\frac{1}{2}\Delta t),\\
K_4 &= F(u(x,0)+\Delta t K_3,\Delta t),\\
w(x,\Delta t) &= w(x,0)+\frac{\Delta t}{6}[K_1+2K_2+2K_3+K_4].
\end{aligned}
\tag{2.17}
$$

Following this evaluation, substitute the determined value of $w(x,\Delta t)$ into Eq (2.15) as a pivotal step in our methodology.

$$
u(x,n\Delta t)=F^{-1}(F(w(x,\Delta t)/(1+ck^4(2\pi/L)^4-ek^2(2\pi/L)^2). \tag{2.18}
$$

To derive the solution $u(x,t)$, Eq (2.12) transforms as follows:

$$
w(x,t+\Delta t)=w(x,t-\Delta t)-2\Delta t(a+b(2\pi/L)^2F^{-1}\{-ik^3F(u)\}+pd(2\pi/L)^{p-1}u^{p-1}(x_j,t)F^{-1}\{ikF(u)\}. \tag{2.19}
$$

In conclusion, we derive the approximate solution by employing the FFT in MATLAB until evaluating $u(x,t)$ at time $t=n\Delta t$, as outlined precisely in Eq (2.7). It's essential to highlight that the central difference method requires us to provide two sets of initial values.

2.3. Algorithm

In this section, we outline the algorithm for the proposed methodology related to the GR-KdV-RLW equation (1.6). The steps below encompass the fundamental components of this approach:

- **Step 1:** Discretize the spatial domain x into spaced grid points.
- **Step 2:** Apply the Fourier derivative theorem to calculate spatial derivatives in Fourier space, then the inverse to get the initial condition.
- **Step 3:** Use the RK4 method to calculate the other initial condition for the central difference method.
- **Step 4:** Thus, we get the solution of (1.6) for various values of N and t.

3. Results and discussion

To assess the effectiveness and precision of the numerical approach, we conducted eight numerical experiments. These experiments included the study of a single solitary wave motion, the interactions of two and interactions of three solitary waves, and the observation of soliton evolution under Gaussian and undular bore initial conditions. This helped us gauge the method's performance and accuracy. To assess solution accuracy, the error norm L_2 is employed, which is defined as [10]:

$$
L_2=\left\|u^{\text{exact}}-u_N\right\|_2\simeq\sqrt{h\sum_{j=1}^{N}\left|u_j^{\text{exact}}-(u_N)_j\right|^2}. \tag{3.1}
$$

Also, utilize the error norm L_∞ for assessing solution accuracy.

$$L_\infty = \left\| u^{\text{exact}} - u_N \right\|_\infty \simeq \max_j |u_j^{\text{exact}} - (u_N)_j|, \quad j = 1, 2, \ldots, N-1. \tag{3.2}$$

To calculate the difference between analytical and numerical solutions at some specified times, the two conserved quantities are given as:

Mass conservation (Lemma 2.1)

$$I_M = \int_a^b u \, \mathrm{d}x \simeq h \sum_{j=1}^{N} u_j^n. \tag{3.3}$$

Energy conservation (Theorem 2.1)

$$I_E(t) = \int_a^b [u^2 + e u_x^2 + c u_{xx}^2] dx \simeq h \sum_{j=1}^{N} [(u_j^n)^2 + e(u_x)_j^n + c(u_{xx})_j^n]. \tag{3.4}$$

The quantities I_M and I_E represent the momentum and energy of the shallow water waves, respectively. Throughout the simulation of solitary wave motion, we observe and track these invariants to evaluate the precision and correctness of the numerical algorithm.

3.1. The motion of the single solitary wave

3.1.1. Example 1

Given the parameters $a = 1, b = 1, c = 1, d = 0.5, e = 0$, and $p = 2$ in Eq (1.6), representing the Rosenau-KdV equation considered with the boundary conditions where $U \to 0$ as $x \to \pm\infty$ to derive the single solitary wave solution:

$$u(x, t) = A \operatorname{sech}^4[B(x - vt)], \tag{3.5}$$

such that

$$A = \frac{210bB^2}{13d}, \quad B = \frac{1}{3}\left[\frac{-13ac + \sqrt{169a^2c^2 + 144b^2c}}{32bc}\right]^{\frac{1}{2}}, \quad v = \frac{b}{52cB^2}. \tag{3.6}$$

The initial condition is as follows:

$$u(x, 0) = A \operatorname{sech}^4(Bx). \tag{3.7}$$

The numerical solutions for a single solitary wave were obtained through the presented method, where $v = 1.18$ considers the variable x within the range $[-70, 100]$. The method exhibits an amplitude of 0.5263 and conducts extensive experimentation when utilizing spatial and temporal step sizes of $\Delta x = 0.1$ and $\Delta t = 0.01$ at time $T = 40$. Figure 1 (a) illustrates a close correspondence between the solitary wave curve and the exact solution. Figure 1 (b), represents the error between the exact and numerical results for solitary waves at time $t = 40$. Figure 2 presents a plan view and a 3D illustration of the motion of a single solitary wave. The method demonstrates the preservation of conserved quantities I_M and I_E, affirming its capability to accurately uphold the soliton's momentum and energy throughout the simulation while maintaining the amplitude remarkably close to its initial

value. Furthermore, Table 1 assesses the performance of the scheme as comparing the error norms L_∞ and L_2 against results obtained from other numerical approaches. As Table 2 shows, the error norms exhibit a significant reduction (halving) as the parameter N increases (doubles). In addition, the numerical invariants closely approach their corresponding analytical values with increasing N, maintaining near-constant values compared to the analytical invariants. The results highlight the superior computational accuracy of the present scheme, as it consistently exhibits the smallest error among the mentioned methods when N increases and Δx, Δt are decreased. These consistently low error values exhibit a high degree of accuracy when compared to alternative methods.

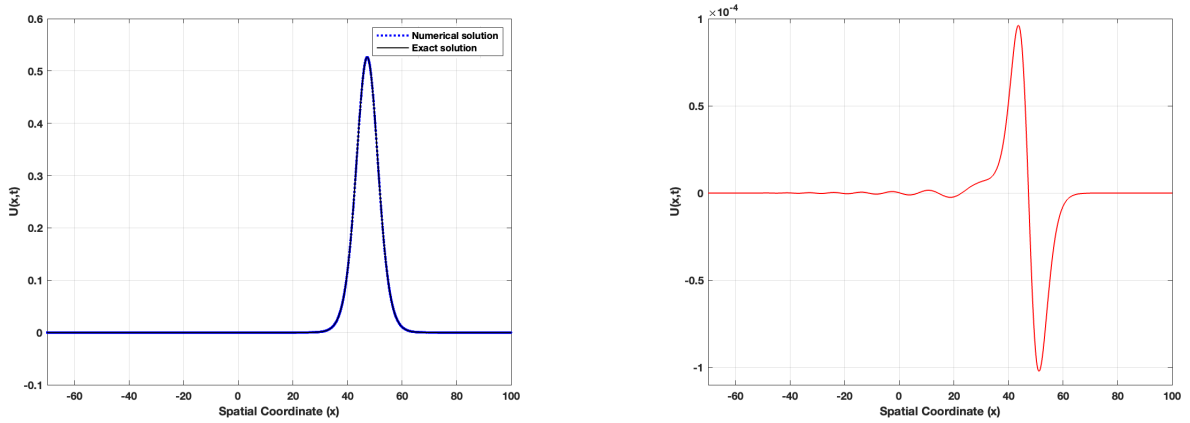

(a) (b)

Figure 1. (a): Motion of a single solitary wave. (b): Error in Example 1 at time $t = 40$ with parameters $N = 32768$, $\Delta x = 0.1$, $\Delta t = 0.01$, $a = 1$, $b = 1$, $c = 1$, $d = 0.5$, $e = 0$, and $x \in [-70, 100]$.

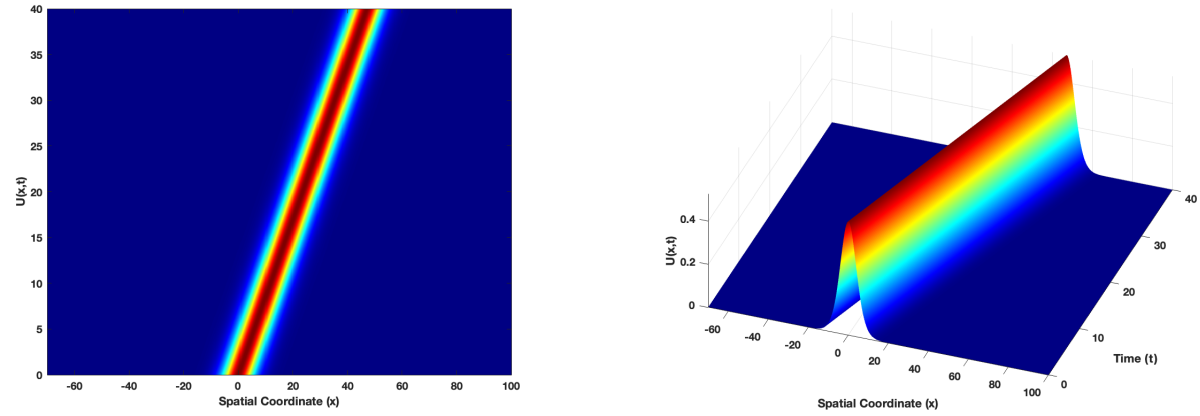

(a) (b)

Figure 2. (a): Plan view of the motion of a single solitary wave. (b): 3D illustration of the motion of a single solitary wave of Example 1 at time $t = 40$ with parameters $N = 32768$, $\Delta x = 0.1$, $\Delta t = 0.01$, $a = 1$, $b = 1$, $c = 1$, $d = 0.5$, $e = 0$, and $x \in [-70, 100]$.

Table 1. The invariants and error norms for the single soliton in Example 1 with specific values, $N = 32768$, $\Delta x = 0.1$, and $\Delta t = 0.01$.

t	I_M	I_E	$L_\infty \times 10^3$	$L_2 \times 10^3$	Amplitude	CPU time (s)
0	5.498005889871813	1.989722881215791	0	0	0.53410	0
10	5.498005889871814	1.989722802347945	0.9323889010	2.9049224720	0.526282	279.2063
20	5.498005889871810	1.989722809878721	0.0505519840	0.1534085381	0.526291	551.0067
30	5.498005889871815	1.989722806497761	0.0763507209	0.2320850336	0.526297	826.4037
40	5.498005889871814	1.989722808570217	0.1022150001	0.3115256472	0.526301	1089.1868
50	5.498005889871809	1.989722808746637	1.0357704951	3.2205212200	0.526314	1357.2288
60	5.498005889871809	1.989722808788525	1.0617460974	3.3008684478	0.526316	1637.9250

Table 2. The invariants and error norms for the single soliton in Example 1 at various N values, assessed at $t = 40$, compared across different methods.

N	Δx	Δt	I_M	I_E	$L_\infty \times 10^3$	$L_2 \times 10^3$
1024	1	0.01	5.492804370581490	1.987861022398681	3.1083809729	9.4207987042
2048	0.1	0.01	5.495489025699077	1.988821936970796	1.5623344409	4.7191964671
4096	0.1	0.01	5.496831353257869	1.989302400117236	0.7835599487	2.3683235481
8192	0.1	0.01	5.497502517037270	1.989542633153467	0.3941988072	1.1928983561
16384	0.1	0.01	5.497838098926962	1.989662750037072	0.1995257407	0.6052412061
32768	0.1	0.01	5.498005889871814	1.989722808570217	0.1022150001	0.3115256472
65536	0.1	0.01	5.498089785344237	1.989752837859619	0.0536065938	0.1648741401
131072	0.1	0.01	5.498131733080447	1.989767852510028	0.0297447895	0.0918889465
131072	0.1	0.1	5.498131733080452	1.989761443558063	0.8287708219	2.2920187254
Comparison of methods						
Sextic B-spline [4]	0.1	0.1	5.4981749335	1.9897841614	0.411492	1.162489
CLDS [8]	0.1	0.1	5.4977342352	1.9847015013	1.878952	5.297873
CFEM [37]	0.1	0.1	5.4981750621	1.9897841635	0.422656	1.187411

3.1.2. Example 2

Given the parameters $a = 1, b = 1, c = 1, d = 1, e = 0$, and $p = 5$ in Eq (1.6) , representing the Rosenau-KdV equation, we have

$$u_t + u_x + (u^5)_x + u_{xxx} + u_{xxxxt} = 0. \tag{3.8}$$

The initial condition was specified as:

$$u_(x, 0) = k_1 \operatorname{sech}(k_2 x). \tag{3.9}$$

This choice yields the exact solitary wave solution:

$$u(x, t) = k_1 \operatorname{sech}[k_2(x - k_3 t)], \tag{3.10}$$

where

$$k_1 = \sqrt[4]{\frac{4}{15}(-5 + \sqrt{34})}, \quad k_2 = \frac{1}{3}\sqrt{-5 + \sqrt{34}}, \quad k_3 = \frac{1}{10}(5 + \sqrt{34}). \tag{3.11}$$

We conducted numerical simulations with specific parameters, considering x within the interval $[-60, 90]$ and $T = 20$. The comparison of the wave graph from the numerical solution is presented in Figure 3. The figure illustrates that the wave amplitude remains nearly identical at different times, suggesting energy conservation. Figure 4 presents a plan view and a 3D illustration of the motion of a single solitary wave. Additionally, a comparison of errors using the L_∞ norm and L_2 norm at $T = 20$ is tabulated in Table 3. Table 4 shows that the error norms exhibit a significant reduction (halving) as the parameter N increases (doubles). Also, it's obvious that the computational efficiency of the new scheme highly surpasses that of the methods presented in the comparison methods when N increases and Δx, Δt are decreased. These results provide strong evidence for the energy conservation property of the new scheme.

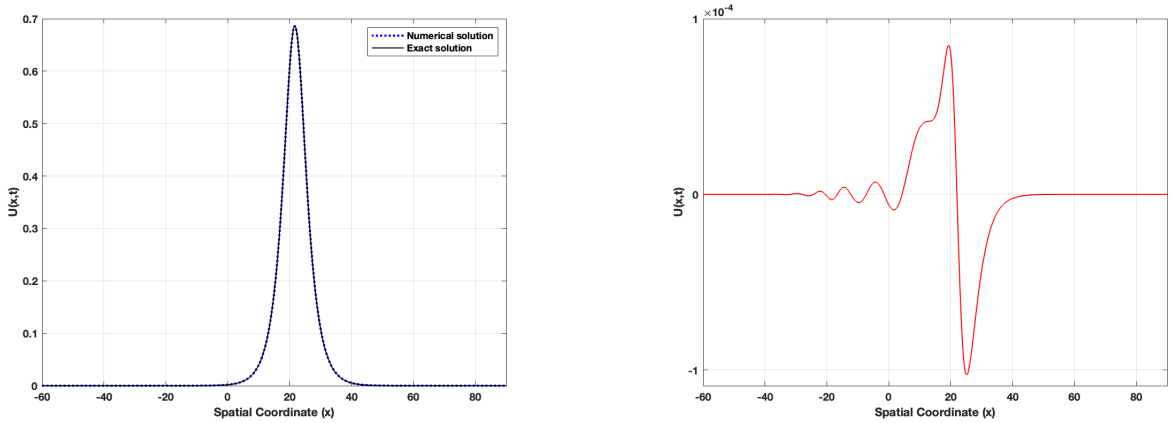

(a) (b)

Figure 3. (a): Motion of single solitary wave. (b): Error of Example 2 at time $t = 20$ with parameters $N = 16384$, $\Delta x = 0.1$, $\Delta t = 0.01$, $a = 1$, $b = 1$, $c = 0$, $d = 1$, $e = 0$, and $x \in [-60, 90]$.

Table 3. Invariants and error norms for the single soliton of Example 2 with $N = 16384$, $\Delta x = 0.1$, and $\Delta t = 0.01$.

t	I_M	I_E	$L_\infty \times 10^3$	$L_2 \times 10^3$	Amplitude
0	7.093210231136498	3.110525454098892	0	0	0.686019
5	7.093210231136510	3.110524968545394	1.1534542328	3.4174191315	0.686072
10	7.093210231136506	3.110525066437504	1.1788351937	3.4911615557	0.686083
15	7.093210231136507	3.110525140466537	1.2038017457	3.5642353055	0.686080
20	7.093210231136505	3.110525118247572	0.1028749227	0.3034375019	0.686074

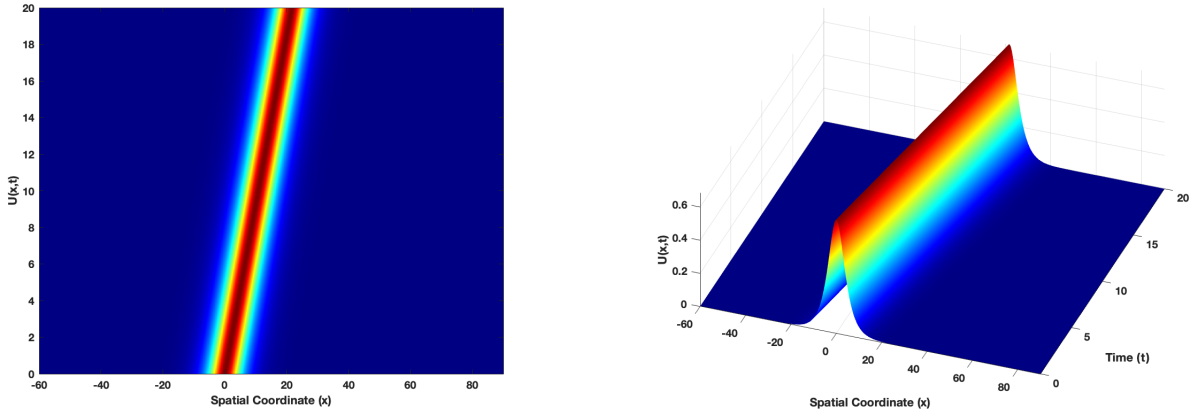

(a) (b)

Figure 4. (a): Plan view of the motion of a single solitary wave. (b): 3D illustration of motion of a single solitary wave of Example 2 at time $t = 20$ with parameters $N = 16384$, $\Delta x = 0.1$, $\Delta t = 0.01$, $a = 1$, $b = 1$, $c = 0$, $d = 1$, $e = 0$, and $x \in [-60, 90]$.

Table 4. Invariants and error norms for the single soliton of Example 2 at different values of N at $t = 20$ comparison with different methods.

N	Δx	Δt	I_M	I_E	$L_\infty \times 10^3$	$L_2 \times 10^3$
2048	0.1	0.01	7.090179499791676	3.109217155558196	0.7916318898	2.3427479567
4096	0.1	0.01	7.091911346274546	3.109964559498229	0.3980440479	1.1772860789
8192	0.1	0.01	7.092777269515867	3.110338264779623	0.2012445858	0.5946188025
16384	0.1	0.01	7.093210231136505	3.110525118247572	0.1028749227	0.3034375019
32768	0.1	0.01	7.093426711946839	3.110618545188292	0.0537538262	0.1581376255
32768	0.1	0.1	7.093426711946828	3.110586752471893	0.8200819099	2.0771466022
Comparison of methods						
[23]	0.1	0.1	-	-	0.18771	0.113342

3.1.3. Example 3

Consider the parameters $a = 1, b = 1, c = 1, d = 1, e = 0$, and $p = 3$ in Eq (1.6), representing the Rosenau-KdV equation so that, the equation takes the following form:

$$u_t + u_x + (u^p)_x + u_{xxx} + u_{xxxxt} = 0, \tag{3.12}$$

which is known as the generalized Rosenau KDV equation and its soliton solution is given in [10]. For $p = 3$, the exact solution is given by:

$$u(x, t) = k_1 \operatorname{sech}^2[k_2(x - k_3 t)], \tag{3.13}$$

where

$$k_1 = \frac{1}{4}\sqrt{-15 + 3\sqrt{41}}, \quad k_2 = \frac{1}{4}\sqrt{\frac{-5 + \sqrt{41}}{2}}, \quad k_3 = \frac{1}{10}(5 + \sqrt{41}). \tag{3.14}$$

The initial condition is

$$u(x, 0) = k_1 \operatorname{sech}^2[k_2 x]. \tag{3.15}$$

Figure 5 displays the comparison of wave amplitude obtained from the numerical solution. The figure reveals that the wave amplitude remains remarkably consistent at different times, implying energy conservation. Furthermore, Figure 6 provides both a plan view and a 3D illustration of the motion of a single solitary wave. Tables 5 provides a comparison of errors using the L_∞ norm and L_2 norm at $T = 40$ for x within the interval $[-60, 90]$. Table 6 shows that the error norms exhibit a significant reduction (halving) as the parameter N increases (doubles). As observed in Tables 5 and 6, the error norms obtained by the method are consistently smaller than those of the other comparison methods when N increases and Δx, Δt are decreased.

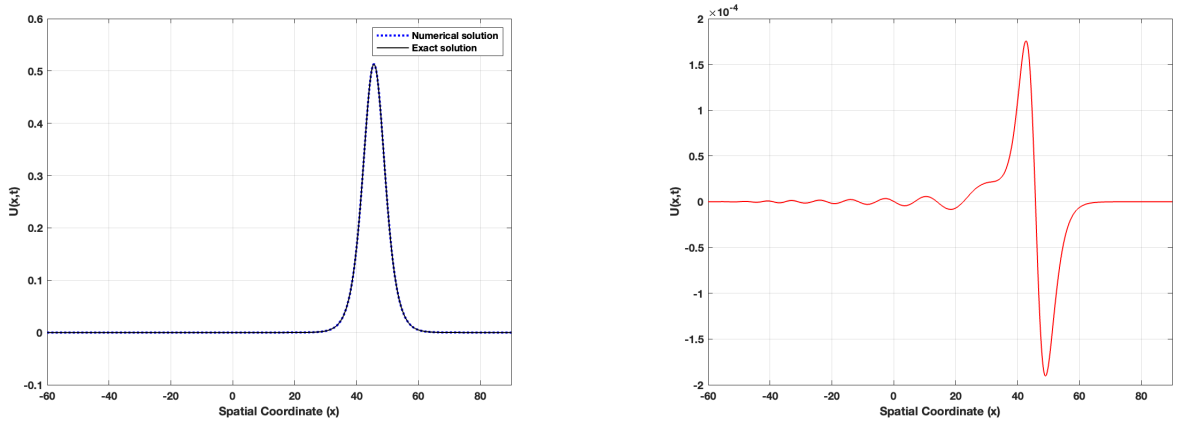

(a) (b)

Figure 5. (a): Motion of single solitary wave. (b): Error of Example 3 at time $t = 40$ with parameters $N = 16384$, $\Delta x = 0.1$, $\Delta t = 0.01$, $a = 1$, $b = 1$, $c = 5$, $d = 1$, $e = 0$, and $x \in [-60, 90]$.

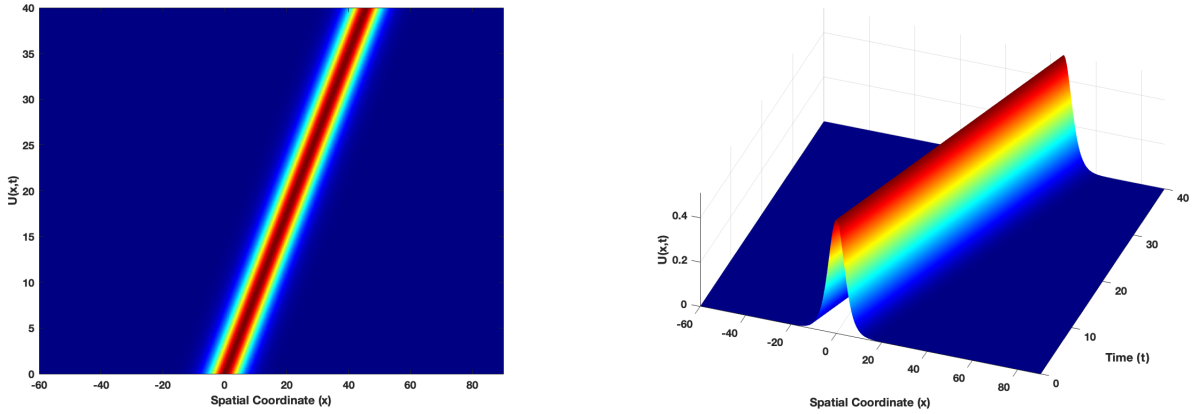

(a) (b)

Figure 6. (a): Plan view of the motion of a single solitary wave.(b): 3D illustration of motion of a single solitary wave of Example 3 at time $t = 40$ with parameters $N = 16384$, $\Delta x = 0.1$, $\Delta t = 0.01$, $a = 1$, $b = 1$, $c = 5$, $d = 1$, $e = 0$, and $x \in [-60, 90]$.

Table 5. Invariants and error norms for the single soliton of Example 3 with $N = 16384$, $\Delta x = 0.1$, and $\Delta t = 0.01$.

t	I_M	I_E	$L_\infty \times 10^3$	$L_2 \times 10^3$	Amplitude
0	4.898680475587986	1.682446890633076	0	0	0.512863
5	4.898680475587988	1.682446669588021	0.9646994328	2.8273426044	0.512883
10	4.898680475587989	1.682446713738066	0.9882448813	2.8930757806	0.512882
15	4.898680475587990	1.682446742297635	1.0120789316	2.9603063735	0.512882
20	4.898680475587982	1.682446732512619	0.0947644616	0.2696706231	0.512862
25	4.898680475587991	1.682446729585691	0.1186665053	0.3380125486	0.512864
30	4.898680475587991	1.682446735013325	0.1425655809	0.4066130028	0.512866
35	4.898680475587989	1.682446742446395	0.1664769241	0.4754175706	0.512867
40	4.898680475587992	1.682446747588404	0.1903588152	0.5443703676	0.512869

Table 6. Invariants and error norms for the single soliton of Example 3 at different values of N at $t = 40$ comparison with different methods.

N	Δx	Δt	I_M	I_E	$L_\infty \times 10^3$	$L_2 \times 10^3$
2048	0.1	0.01	4.896587405739421	1.681740472990474	1.4742529842	4.2031274345
4096	0.1	0.01	4.897783445652888	1.682144056497737	0.7406123146	2.1124065578
8192	0.1	0.01	4.898381465609623	1.682345850228840	0.3737781703	1.0670058118
16384	0.1	0.01	4.898680475587992	1.682446747588404	0.1903588152	0.5443703676
32768	0.1	0.01	4.898829980577171	1.682497196391648	0.0986916137	0.2832076016
32768	0.1	0.5	4.898829980576815	1.682790870144930	26.0471738546	69.8929283038
32768	0.1	0.25	4.898829980577174	1.682445210448126	6.3340343984	17.0588205575
32768	0.1	0.0625	4.898829980577184	1.682491883652615	0.4652663223	1.2625554515
Comparison of methods						
[13] 2M = 128	-	0.5	-	-	4.85593	1.18987
[13] 2M = 128	-	0.25	-	-	0.62532	0.1592
[38] N = 200	-	0.25	-	-	9.9701002	26.393848
[38] N = 600	-	0.0625	-	-	0.61045529	1.6159943

3.1.4. Example 4

In this example, considering the parameters $a = 1, b = 1, c = 1, d = 0.5, e = 1$, and $p = 2$, Eq (1.6) becomes

$$u_t + u_x + 0.5(u^2)_x - u_{xxt} + u_{xxx} + u_{xxxxt} = 0. \tag{3.16}$$

The exact solution of the equation is

$$u(x,t) = k_1 \operatorname{sech}^4[k_2(x - k_3 t)], \tag{3.17}$$

where

$$k_1 = \frac{-5(25 - 13\sqrt{457})}{456}, \quad k_2 = \frac{\sqrt{-13 + \sqrt{457}}}{\sqrt{288}}, \quad k_3 = \frac{241 + 13\sqrt{457}}{266}. \tag{3.18}$$

The initial condition is defined as:

$$u(x,0) = k_1 \operatorname{sech}^4[(k_2 x)]. \tag{3.19}$$

In Figure 7, the numerical solutions closely match the exact solutions. These figures demonstrate that the wave amplitude at various time instances remains nearly constant. Figure 8 provides both a plan view and a 3D illustration of the motion of a single solitary wave. Furthermore, the error norms L_∞ and L_2 at time $T = 30$ for x within the interval $[-40, 100]$ are summarized in Table 7. It is observed from Table 8 that the errors are significantly reduced (halved) as the parameter N increases (doubles), and the resulting error norms are notably good, being smaller than those of the compared methods when N increases and Δx, Δt are decreased.

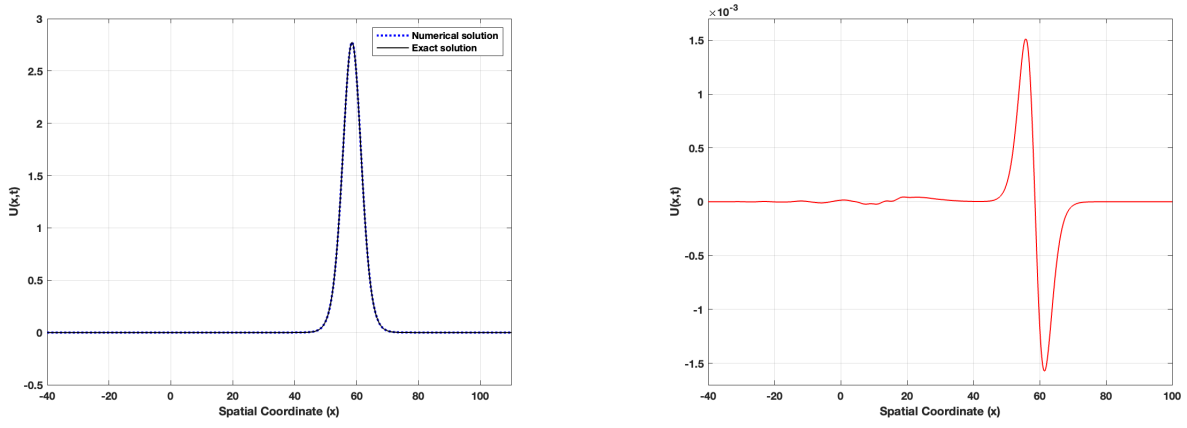

(a) (b)

Figure 7. (a): Motion of single solitary wave. (b): Error of Example 4 at time $t = 30$ with parameters $N = 16384$, $\Delta x = 0.1$, $\Delta t = 0.01$, $a = 1$, $b = 1$, $c = 1$, $d = 0.5$, $e = 1$, and $x \in [-40, 100]$.

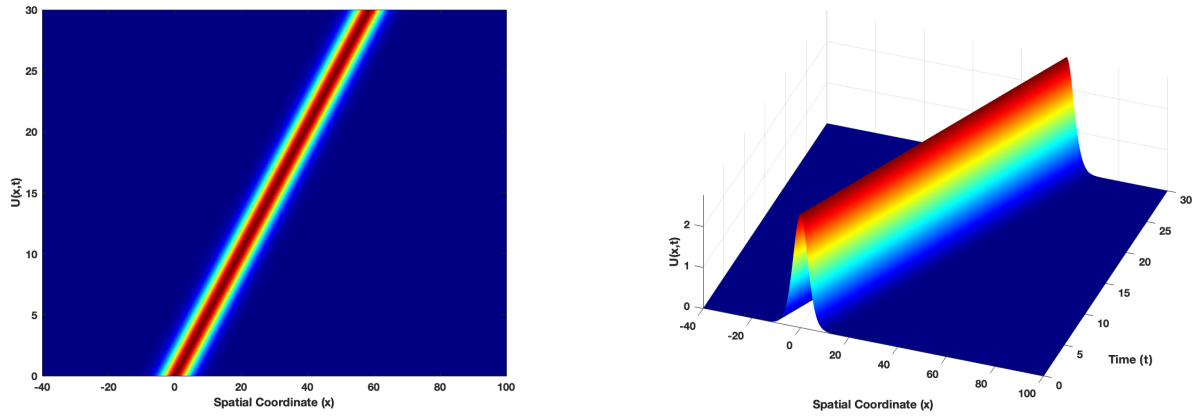

(a) (b)

Figure 8. (a): Plan view of the motion of a single solitary wave. (b): 3D illustration of motion of a single solitary wave of Example 4 at time $t = 30$ with parameters $N = 16384$, $\Delta x = 0.1$, $\Delta t = 0.01$, $a = 1$, $b = 1$, $c = 1$, $d = 0.5$, $e = 1$, and $x \in [-40, 100]$.

Table 7. Invariants and error norms for the single soliton of Example 4 with $N = 16384$, $\Delta x = 0.1$, and $\Delta t = 0.01$.

t	I_M	I_E	$L_\infty \times 10^3$	$L_2 \times 10^3$	Amplitude
0	21.677935246115432	43.714878717385488	0	0	2.772714
10	21.677935246115425	43.714739731779780	11.0692526920	29.7777663315	2.772978
20	21.677935246115439	43.714742070342737	1.0407675579	2.7303206997	2.772863
30	21.677935246115450	43.714742083338137	1.5730326889	4.1630128166	2.772940
40	21.677935246115425	43.714742085532912	2.1054700713	5.5983379261	2.772997
50	21.677935246115435	43.714742085120818	13.1996093543	35.5139206988	2.773050
60	21.677935246115425	43.714742085181292	13.7318973109	36.9511529697	2.773022

Table 8. Invariants and error norms for the single soliton of Example 4 at different values of N at $t = 30$ comparison with different methods.

N	Δx	Δt	I_M	I_E	$L_\infty \times 10^3$	$L_2 \times 10^3$
2048	0.1	0.01	21.668672867630249	43.698502820622423	11.5622347894	30.1801854595
4096	0.1	0.01	21.673965655336072	43.707782207037859	5.8537655004	15.3122195433
8192	0.1	0.01	21.676612049188961	43.712422092540535	2.9998722998	7.8784632887
16384	0.1	0.01	21.677935246115450	43.714742083338137	1.5730326889	4.1630128166
32768	0.1	0.01	21.678596844578685	43.715902090745146	0.8598416802	2.3078805322
32768	0.125	0.125	21.678596844578667	43.695652293217044	31.3914760561	77.6256082731
Comparison of methods						
Lie–Trotter [21]	0.125	0.125	-	-	8.72888	28.9336
Strang [21]	0.125	0.125	-	-	9.33938	24.1393
[39]	0.125	0.125	-	-	214.488	805.629
[23]	0.125	0.125	-	-	197.127	518.662

3.2. Interaction of two solitary waves

3.2.1. Example 5

To simulate the interaction between two solitary waves, consider the Eq (1.6) with the following parameters $a = 1$, $b = 1$, $c = 1$, $d = 0.5$, $e = 0$, $h = 0.1$, $\Delta t = 0.01$, $v_1 = 0.3$, $v_2 = 0.5$, $x_1 = -70$, and $x_2 = -35$ across the spatial domain $x \in [-100, 400]$, which represents the Rosenau-KdV equation. The initial condition, defined as the linear sum of two well-separated solitary waves with different amplitudes, is expressed as:

$$u(x, 0) = \sum_{i=1}^{2} A_i \operatorname{sech}^4[B_i(x - x_i)], \tag{3.20}$$

such that

$$A_i = \frac{210bB_i^2}{13d}; \quad B_i = \left| \sqrt{\frac{b}{52cV_i}} \right|; \quad i = 1, 2, \tag{3.21}$$

where v_i and x_i are constants. The experiment was conducted up to $t = 250$ for parameters $N = 8192$, illustrating the interaction of two solitary waves at different times, as depicted in Figure 9. The waves originate from positions $x = -70$ and $x = -35$ from left to right, respectively. The taller wave, characterized by a larger amplitude, travels faster than the one with a smaller amplitude. At $t = 80$, the taller wave catches up to the smaller one and merges with it. Two waves interact until around $t = 130$, and this interaction extends until $t = 150$. By $t = 250$, the interaction concludes, and the larger soliton has fully separated. Following this interaction, the waves retain their original shapes and amplitudes. Figure 10 presents a plan view and a 3D illustration of the interaction of two solitary waves. The values of the conserved quantities are denoted as I_M and I_E and have been determined and listed in Table 9. The simulation showed that the invariants remained nearly constant over time.

Table 9. The conserved quantities during the interaction of two solitary waves in Example 5 with $a = 1$, $b = 1$, $c = 1$, $d = 0.5$, $e = 0$, $h = 0.1$, $\Delta t = 0.01$, $v_1 = 0.3$, $v_2 = 0.5$, $x_1 = -70$, and $x_2 = -35$, over the domain $-100 \leq x \leq 400$.

t	I_M	I_E
0	19.352141010394462	23.452728190236975
50	19.352141010394472	23.452601901412166
100	19.352141010394458	23.452555193310442
150	19.352141010394476	23.452595067709840
200	19.352141010394465	23.452597162759467
250	19.352141010394451	23.452597166369134

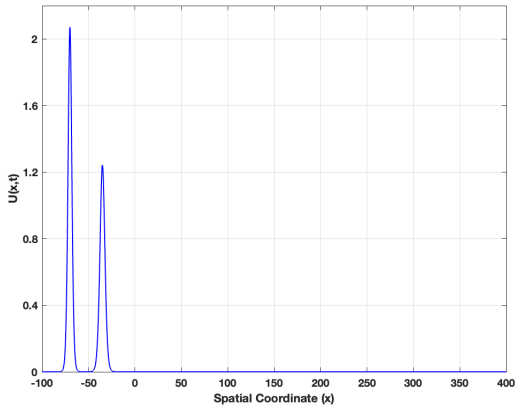

(t=0)

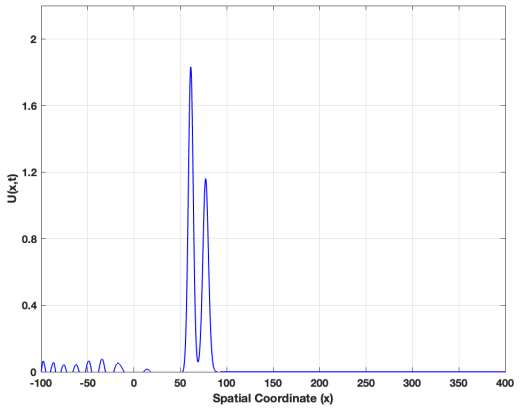

(t=80)

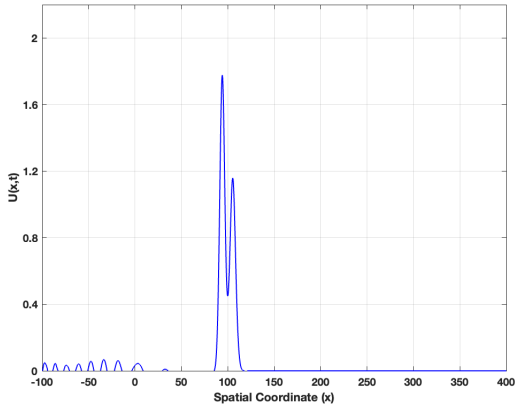

(t=100)

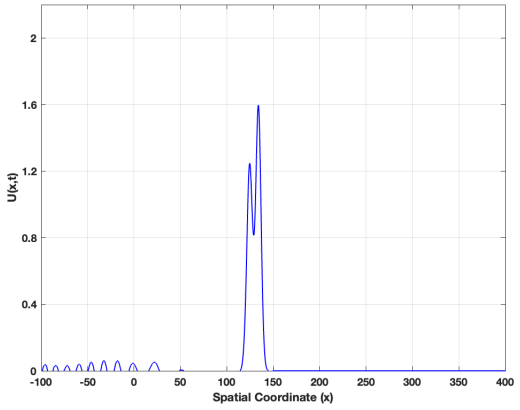

(t=120)

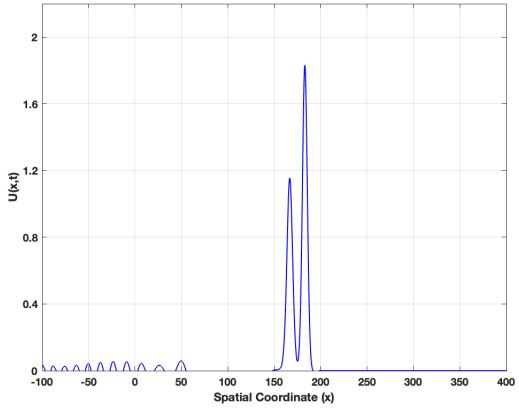

(t=150)

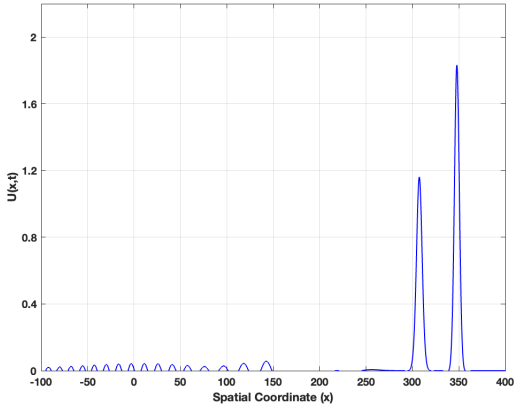

(t=250)

Figure 9. Interaction between two solitary waves in Example 5 with $a = 1, b = 1, c = 1, d = 0.5, e = 0, v1 = 0.3, v2 = 0.5, x1 = -70, x2 = -35, N = 8192, \Delta x = 0.1$, and $\Delta t = 0.01$.

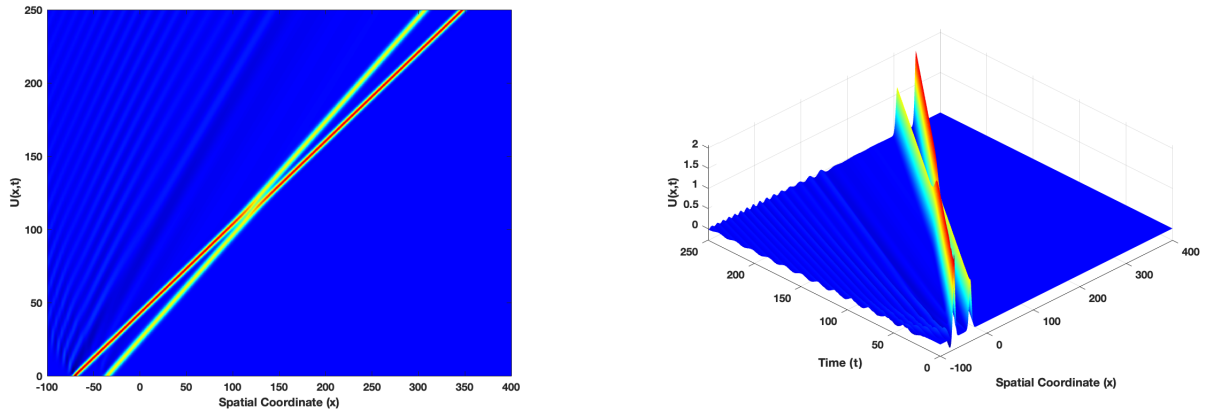

(a) (b)

Figure 10. (a): Plan view of the interaction between two solitary waves. (b): 3D illustration between the interaction of two solitary waves of Example 5 with $a = 1, b = 1, c = 1, d = 0.5, e = 0, v1 = 0.3, v2 = 0.5, x1 = -70, x2 = -35, N = 8192, \Delta x = 0.1$, and $\Delta t = 0.01$.

3.3. Interaction of three solitary waves

3.3.1. Example 6

To simulate the interaction of three solitary waves with different amplitudes, consider the Eq (1.6) with the following parameters $a = 1$, $b = 1$, $c = 1$, $d = 0.5$, $e = 0$, $h = 0.1$, $\Delta t = 0.1$, $v_1 = 0.3$, $v_2 = 0.5$, $v_3 = 0.8$, $x_1 = -70$, $x_2 = -40$, and $x_3 = -15$ over the spatial domain $x \in [-100, 400]$, which represents the Rosenau-KdV equation, and set an initial condition as follows:

$$u(x, 0) = \sum_{i=1}^{3} A_i \operatorname{sech}^4[B_i(x - x_i)]. \tag{3.22}$$

The parameters A_i, B_i, and i are defined as follows:

$$A_i = \frac{210bB_i^2}{13d}; \quad B_i = \left|\sqrt{\frac{b}{52cv_i}}\right|; \quad i = 1, 2, 3, \tag{3.23}$$

such that v_i and x_i are constants. The simulation is conducted up to time $t = 250$, and our proposed algorithm is executed with $N = 8192$. In Figure 11, the results are illustrated at various time intervals. These waves travel from left to right, and each has a distinct velocity. The figure shows that the tallest wave, characterized by a larger amplitude, moves faster than the smaller waves. The interaction starts at $t = 50$ and persists until around $t = 170$. Throughout this period, the taller wave engages with the two shorter waves reciprocally, and the shorter waves also interact with each other before eventually separating. After this interaction, the waves progress while preserving their original shapes and amplitudes, even after the simulation time of $t = 250$. Figure 12 presents a plan view and a 3D illustration of the interaction of three solitary waves. Table 10 presents the values of conserved quantities throughout the simulation. It is obvious from Table 10 that the calculated invariants maintain remarkable stability during the entire computational process.

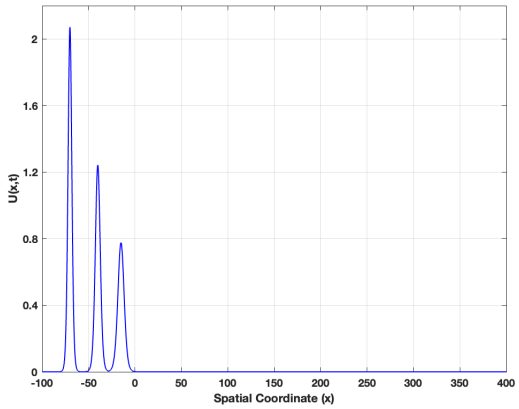

(t=0)

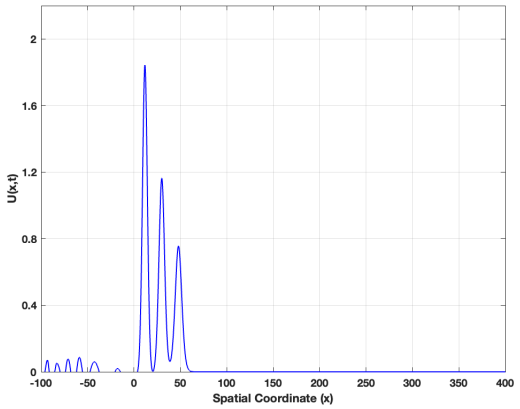

(t=50)

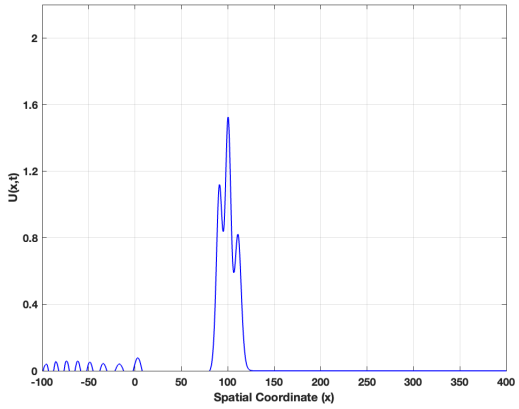

(t=100)

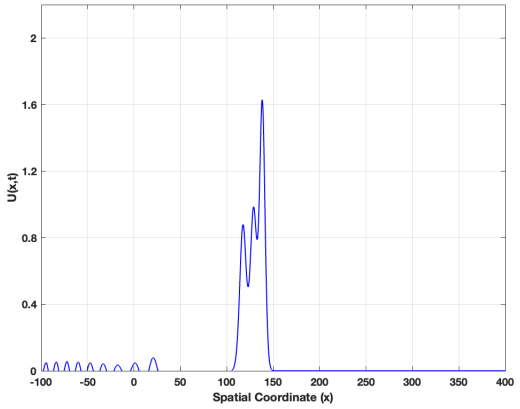

(t=120)

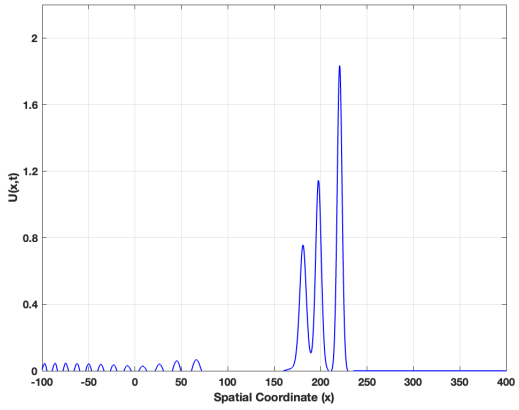

(t=170)

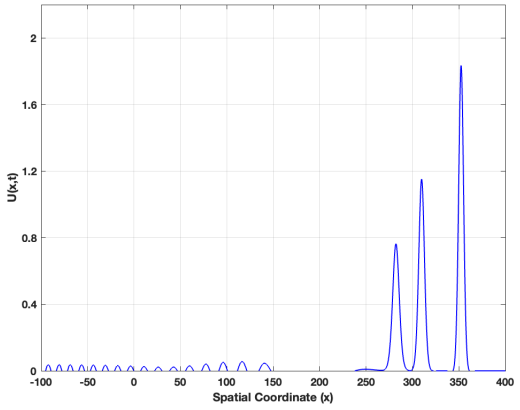

(t=250)

Figure 11. Thes interaction of the three solitary waves in Example 6 with $a = 1$, $b = 1$, $c = 1$, $d = 0.5$, $e = 0$, $h = 0.1$, $\Delta t = 0.01$, $v_1 = 0.3$, $v_2 = 0.5$, $v_3 = 0.8$, $x_1 = -70$, $x_2 = -40$, $x_3 = -15$, and $x \in [-100, 400]$ at selected times.

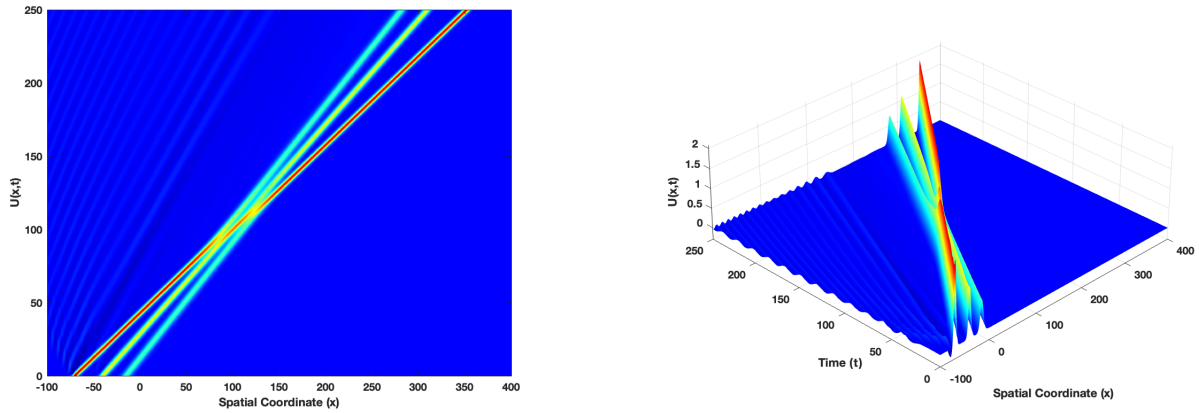

(a) (b)

Figure 12. (a): Plan view of the interaction of three solitary waves. (b): 3D illustration of the interaction among three solitary waves of Example 6 with $a = 1$, $b = 1$, $c = 1$, $d = 0.5$, $e = 0$, $h = 0.1$, $\Delta t = 0.01$, $v_1 = 0.3$, $v_2 = 0.5$, $v_3 = 0.8$, $x_1 = -70$, $x_2 = -40$, $x_3 = -15$, and $x \in [-100, 400]$.

Table 10. The conserved quantities during the interaction of the three solitary waves in Example 6 with $a = 1$, $b = 1$, $c = 1$, $d = 0.5$, $e = 0$, $h = 0.1$, $\Delta t = 0.01$, $v_1 = 0.3$, $v_2 = 0.5$, $v_3 = 0.8$, $x_1 = -70$, $x_2 = -40$, $x_3 = -15$, and $-100 \leq x \leq 400$.

t	I_M	I_E
0	26.030119128954244	27.030613490768943
50	26.030119128954254	27.030484481965665
100	26.030119128954261	27.030335144434130
150	26.030119128954251	27.030471130701706
200	26.030119128954233	27.030480691407945
250	26.030119128954254	27.030481153013991

3.4. Evolution of solitons

3.4.1. Example 7: Gaussian initial condition

The evolution of a train of solitons is governed by Eq (1.6) with the following parameters $a = 1, b = 1$, $d = 0.5$, and $e = 0$, which represents the Rosenau-KdV equation. The development of a train of solitons determined by the Rosenau-KdV equation will be evaluated using a Gaussian initial condition:

$$u(x, 0) = \exp[-(x - 40)^2]. \tag{3.24}$$

Consider the boundary condition as:

$$u(-50, t) = u(250, t), \quad t > 0. \tag{3.25}$$

To explore the behavior of the solution for different values of c, consider the impact of these particular c values on its dependence, $c = 0.5, 0.1, 0.05$, and 0.01, $h = 0.1$, $\Delta t = 0.01$, within the time

interval $0 \leq t \leq 14$, and over the spatial domain $x \in [-50, 250]$. The numerical computations are performed up to $t = 14$. Figure 13 displays the evolution of the Gaussian initial condition into solitons at $t = 10$. The values of the two invariants of motion are presented in Table 11 for different c values, illustrating the constancy of these invariants as time advances. This demonstrates the presence of oscillating solitons, and the number of oscillating solitons depends on the value of c. A decrease in the value of c leads to an increase in the number of oscillating solitons.

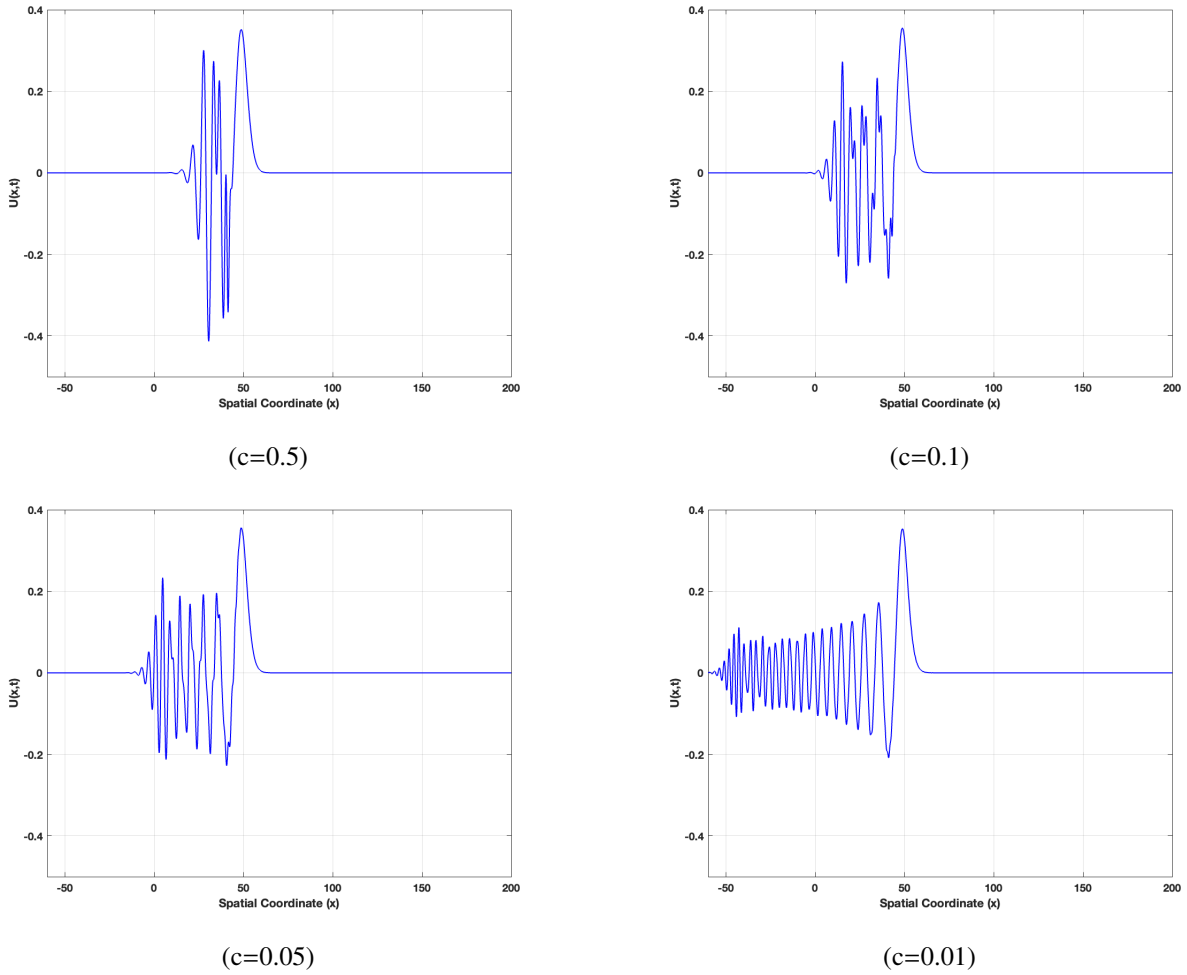

Figure 13. Waves resulting from the Gaussian initial condition described in Example 7 with $a = 1$, $b = 1$, $d = 0.5$, $e = 0$, $v = 1.18$, $h = 0.1$, $\Delta t = 0.01$, $x \in [-50, 250]$, and different values of c at $t = 10$.

Table 11. Invariants associated with the Gaussian initial condition, as in Example 7, across various values of c at $0 \leq t \leq 14$, with $a = 1$, $b = 1$, $d = 0.5$, $e = 0$, $v = 1.18$, $h = 0.1$, $\Delta t = 0.01$, $-50 \leq x \leq 250$.

	$c = 0.5$		$c = 0.1$	
t	I_M	I_E	I_M	I_E
0	1.772237486910044	3.133820984974885	1.772237486910044	1.629293112888655
2	1.772237486910047	3.133237313798476	1.772237486910045	1.628721098523413
4	1.772237486910043	3.133573315250525	1.772237486910043	1.628819101869206
6	1.772237486910044	3.133132582210868	1.772237486910043	1.628989812794706
8	1.772237486910046	3.133625933359089	1.772237486910046	1.628971191156475
10	1.772237486910045	3.133332831613470	1.772237486910045	1.628947943212157
12	1.772237486910043	3.133416253582500	1.772237486910044	1.628938811401362
14	1.772237486910046	3.133438843929645	1.772237486910043	1.628938774175789
	$c = 0.05$		$c = 0.01$	
	I_M	I_E	I_M	I_E
0	1.772237486910044	1.441227128877877	1.772237486910044	1.290774341669254
2	1.772237486910043	1.440883444814180	1.772237486910045	1.290621937574925
4	1.772237486910043	1.441009452846298	1.772237486910045	1.290609096773492
6	1.772237486910046	1.441013586107876	1.772237486910043	1.290625441218467
8	1.772237486910045	1.440970135019521	1.772237486910046	1.290632027428226
10	1.772237486910045	1.440932082819944	1.772237486910043	1.290623276335061
12	1.772237486910044	1.440929794432098	1.772237486910046	1.290621153719395
14	1.772237486910043	1.440921837459404	1.772237486910046	1.290627760084339

3.4.2. Example 8: Undular bore initial condition

For the evolution of a train of solitons, consider the Eq (1.6) with the following parameters $a = 1$, $b = 1$, $c = 1$, $d = 0.5$, $e = 0$, $v = 1.18$, $h = 0.1$, $\Delta t = 0.01$, $u_0 = 1$, $x_0 = 25$, and $d = 5$, which represents the Rosenau-KdV equation. The equation is examined utilizing the undular bore initial condition expressed as:

$$u(x, 0) = \frac{1}{2}u_0[1 - \tanh(\frac{|x| - x_0}{d})]. \tag{3.26}$$

The provided boundary condition is expressed as:

$$u(-50, t) = u(350, t), \quad t > 0. \tag{3.27}$$

To investigate the generation of a train of solitons within the Rosenau-KdV, we examine the impact of parameter c. These solitons represent an undular bore, which reflects the water's surface above the equilibrium level at $t = 0$. The computational simulation runs until time $t = 150$. Figure 14 displays that simulation reveals the transformation of the initial perturbation into a train of solitons at specific time intervals. Over time, the evolution becomes evident as six solitons propagate to the right. The numerical results, which include two conserved quantities, are presented in Table 12, showing that these quantities are preserved.

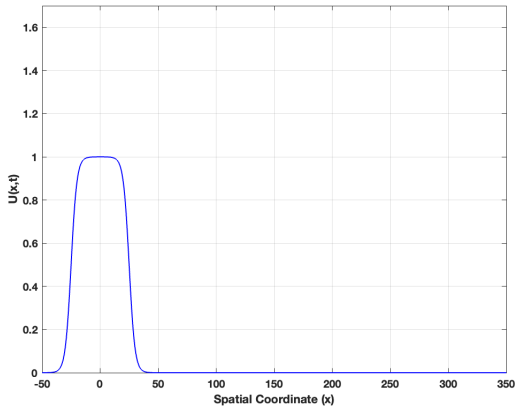

(t=0)

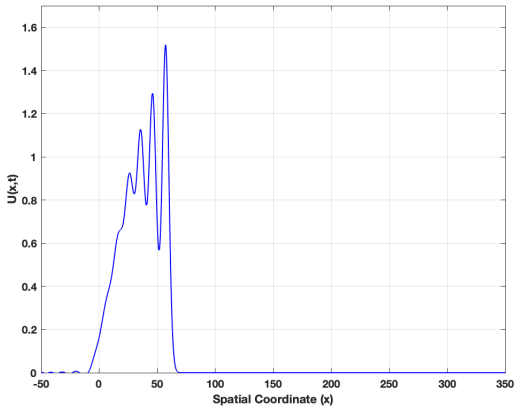

(t=25)

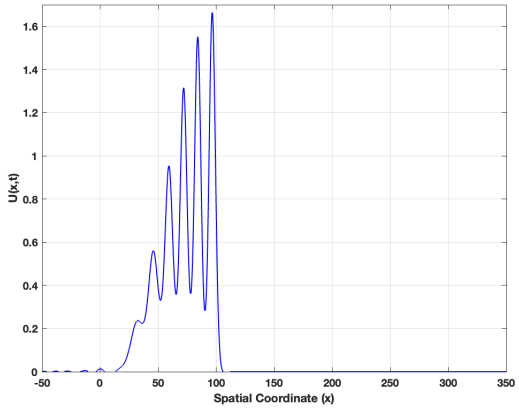

(t=50)

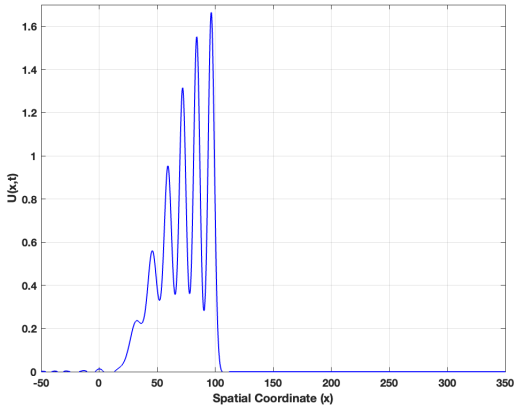

(t=75)

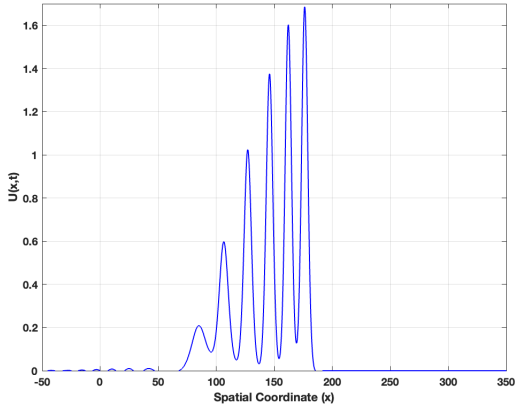

(t=100)

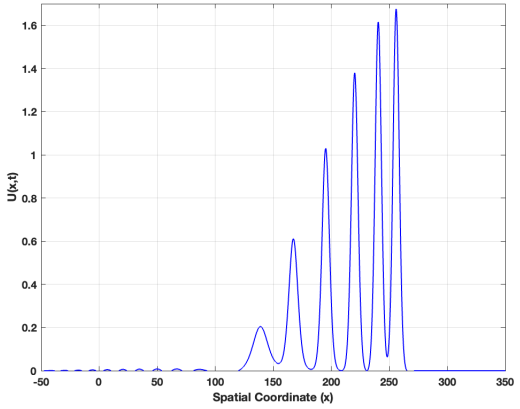

(t=150)

Figure 14. Developed train solitons for undular bore initial condition of Example 8 at selected times with $v = 1.18, h = 0.1, \Delta t = 0.01, a = 1, b = 1, c = 1, d = 0.5, e = 0$, and $x \in [-50, 350]$.

Table 12. Invariants associated with the undular bore initial condition as in Example 8 with $v = 1.18$, $h = 0.1$, $\Delta t = 0.01$, $a = 1$, $b = 1$, $c = 1$, $d = 0.5$, $e = 0$, and $x \in [-50, 350]$ at $t \in [0, 150]$.

t	I_M	I_E
0	49.994123436028708	44.999228972625303
25	49.994123436028701	44.999321125767089
50	49.994123436028737	44.999466996781024
75	49.994123436028701	44.999526896758091
100	49.994123436028701	44.999544395471474
125	49.994123436028723	44.999553042657546
150	49.994123436028715	44.999552868273128

4. Conclusions

This article presents a combination of the Fourier spectral method and the central difference method. The accuracy and efficiency of the combined scheme were assessed by computing error norms and conservation properties related to the GR-KDV-RLW equation. The numerical results obtained are satisfactory and comparable to other solutions in the literature. The approach exhibits better accuracy compared to the previously presented results when N increases and Δx, Δt are decreased. Furthermore, our method can be applied to similar types of PDEs that model real-life problems, which makes it useful for further research in various scientific fields, such as materials science and engineering.

Use of AI tools declaration

The authors declare that they have not used Artificial Intelligence (AI) tools in the creation of this article.

Conflict of interest

The authors declare that they have no conflicts of interest.

References

1. T. R. Marchant, Asymptotic Solitons for a Higher-Order Modified Korteweg–de Vries Equation, *Phys. Rev. E*, **66** (2002), 046623. https://doi.org/10.1103/PhysRevE.66.046623
2. D. Kordeweg, G. de Vries, On the Change of Form of Long Waves Advancing in a Rectangular Channel, and a New Type of Long Stationary Wave, *Philos. Mag.*, **39** (1895), 422–443. https://doi.org/10.1080/14786449508620739
3. Z. Feng, On Travelling Wave Solutions of the Burgers–Korteweg–de Vries Equation, *Nonlinearity*, **20** (2007), 343. http://doi.org/10.1088/0951-7715/20/2/006

4. T. Ak, S. B. G. Karakoc, H. Triki, Numerical Simulation for Treatment of Dispersive Shallow Water Waves with Rosenau-KdV Equation, *Eur. Phys. J. Plus*, **131** (2016), 356. https://doi.org/10.1140/epjp/i2016-16356-3
5. P. Rosenau, Dynamics of Dense Discrete Systems: High Order Effects, *Prog. Theor. Phys.*, **79** (1988), 1028–1042. http://doi.org/10.1143/PTP.79.1028
6. P. Rosenau, A Quasi-continuous Description of a Nonlinear Transmission Line, *Phys. Scr.*, **34** (1986), 827. http://doi.org/10.1088/0031-8949/34/6B/020
7. J.-M. Zuo, Solitons and Periodic Solutions for the Rosenau–KdV and Rosenau–Kawahara Equations, *Appl. Math. Comput.*, **215** (2009), 835–840. http://doi.org/10.1016/j.amc.2009.06.011
8. J. Hu, Y. Xu, B. Hu, Conservative Linear Difference Scheme for Rosenau-KdV Equation, *Adv. Math. Phys.*, **2013** (2013), 423718. https://doi.org/10.1155/2013/423718
9. H. Ahmad, T. A. Khan, S.-W. Yao, An Efficient Approach for the Numerical Solution of Fifth-Order KdV Equations, *Open Math.*, **18** (2020), 738–748. https://doi.org/10.1515/math-2020-0036
10. A. Esfahani, Solitary Wave Solutions for Generalized Rosenau-KdV Equation, *Commun. Theor. Phys.*, **55** (2011), 396–398. https://doi.org/10.3390/math8091601
11. A. Ghiloufi, K. Omrani, New Conservative Difference Schemes with Fourth-Order Accuracy for Some Model Equation for Nonlinear Dispersive Waves, *Numer. Meth. Part. D. E.*, **34** (2018), 451–500. http://doi.org/10.1002/num.22208
12. P. Razborova, L. Moraru, A. Biswas, Perturbation of Dispersive Shallow Water Waves with Rosenau-KdV-RLW Equation and Power Law Nonlinearity, *Rom. J. Phys*, **59** (2014), 658–676.
13. A. K. Verma, M. K. Rawani, Numerical Solutions of Generalized Rosenau–KDV–RLW Equation by Using Haar Wavelet Collocation Approach Coupled with Nonstandard Finite Difference Scheme and Quasilinearization, *Numer. Meth. Part. D. E.*, **39** (2023), 1085–1107. http://doi.org/10.1002/num.22925
14. W. Zhao, G.-R. Piao, A Reduced Galerkin Finite Element Formulation Based on Proper Orthogonal Decomposition for the Generalized KDV-RLW-Rosenau Equation, *J. Inequal. Appl.*, **2023** (2023), 104. http://doi.org/10.1186/s13660-023-03012-1
15. M. Ahmat, J. Qiu, SSP IMEX Runge-Kutta WENO Scheme for Generalized Rosenau-KdV-RLW Equation, *J. Math. Study*, **55** (2022), 1–21. http://doi.org/10.4208/jms.v55n1.22.01
16. S. Özer, Two Efficient Numerical Methods for Solving Rosenau-KdV-RLW Equation, *Kuwait J. Sci.*, **48** (2021), 14–24. https://doi.org/10.48129/kjs.v48i1.8610
17. Z. Avazzadeh, O. Nikan, J. A. T. Machado, Solitary Wave Solutions of the Generalized Rosenau-KdV-RLW Equation, *Mathematics*, **8** (2020), 1601. http://doi.org/10.3390/math8091601
18. Shallu, V. Kukreja, An Efficient Collocation Algorithm with SSP-RK43 to Solve Rosenau-KdV-RLW Equation, *Int. J. Appl. Comput. Math.*, **7** (2021), 161. http://doi.org/10.1007/s40819-021-01095-2
19. S. B. G. Karakoç, A New Numerical Application of the Generalized Rosenau-RLW Equation, *Sci. Iran.*, **27** (2020), 772–783. http://doi.org/10.24200/sci.2018.50490.1721

20. C. Guo, F. Li, W. Zhang, Y. Luo, A Conservative Numerical Scheme for Rosenau-RLW Equation Based on Multiple Integral Finite Volume Method, *Bound. Value Probl.*, **2019** (2019), 168. http://doi.org/10.1186/s13661-019-1273-2

21. S. Özer, Numerical Solution of the Rosenau–KdV–RLW Equation by Operator Splitting Techniques Based on B-spline Collocation Method, *Numer. Meth. Part. D. E.*, **35** (2019), 1928–1943. https://doi.org/10.1002/num.22387

22. S. Özer, An Effective Numerical Technique for the Rosenau-KdV-RLW Equation, *Balıkesir Üniversitesi Fen Bilimleri Enstitüsü Dergisi*, **20** (2018), 1–14. http://doi.org/10.25092/baunfbed.475968

23. X. Wang, W. Dai, A Three-Level Linear Implicit Conservative Scheme for the Rosenau–KdV–RLW Equation, *J. Comput. Appl. Math.*, **330** (2018), 295–306. https://doi.org/10.1016/j.cam.2017.09.009

24. Y. Gong, Q. Wang, Y. Wang, J. Cai, A Conservative Fourier Pseudo-Spectral Method for the Nonlinear Schrödinger Equation, *J. Comput. Phys.*, **328** (2017), 354–370. https://doi.org/10.1016/j.jcp.2016.10.022

25. S. Akter, M. S. Mahmud, M. Kamrujjaman, H. Ali, Spectral Collocation Method with Fourier Transform to Solve Differential Equations, *GANIT J. Bangladesh Math. Soc.*, **40** (2020), 28–42. https://doi.org/10.3329/ganit.v40i1.48193

26. L. Zhang, W. Yang, X. Liu, H. Qu, Fourier Spectral Method for a Class of Nonlinear Schrödinger Models, *Adv. Math. Phys.*, **2021** (2021), 9934858. https://doi.org/10.1155/2021/9934858

27. R. Zheng, X. Jiang, Spectral Methods for the Time-Fractional Navier–Stokes Equation, *Appl. Math. Lett.*, **91** (2019), 194–200. https://doi.org/10.1016/j.aml.2018.12.018

28. H. N. Hassan, An Efficient Numerical Method for the Modified Regularized Long Wave Equation Using Fourier Spectral Method, *J. Assoc. Arab Univ. Basic Appl. Sci.*, **24** (2017), 198–205. http://doi.org/10.1016/j.jaubas.2016.10.002

29. Z. Cai, B. Lin, M. Lin, A Positive and Moment-Preserving Fourier Spectral Method, 2023, arXiv:2304.11847. https://doi.org/10.48550/arXiv.2304.11847

30. R. Zheng, X. Jiang, H. Zhang, L1 Fourier Spectral Methods for a Class of Generalized Two-Dimensional Time Fractional Nonlinear Anomalous Diffusion Equations, *Comput. Math. Appl.*, **75** (2018), 1515–1530. https://doi.org/10.1016/j.camwa.2017.11.017

31. H. N. Hassan, Numerical Solution of a Boussinesq Type Equation Using Fourier Spectral Methods, *Zeitschrift für Naturforschung A*, **65** (2010), 305–314. http://dx.doi.org/10.1515/zna-2010-0407

32. H. N. Hassan, H. K. Saleh, The Solution of the Regularized Long Wave Equation Using the Fourier Leap-Frog Method, *Zeitschrift für Naturforschung A*, **65** (2010), 268–276. https://doi.org/10.1515/zna-2010-0402

33. H. N. Hassan, An Accurate Numerical Solution for the Modified Equal Width Wave Equation Using the Fourier Pseudo-Spectral Method, *J. Appl. Math. Phys.*, **4** (2016), 1054–1067. https://doi.org/10.4236/jamp.2016.46110

34. A. P. Harris, T. A. Biala, A. Q. M. Khaliq, Fourier Spectral Methods with Exponential Time Differencing for Space-Fractional Partial Differential Equations in Population Dynamics, 2022, arXiv:2212.03345. https://doi.org/10.48550/arXiv.2212.03345

35. N. Yizengaw, Convergence Analysis of Finite Difference Method for Differential Equation, *J. Phys. Math.*, **8** (2017), 240. https://doi.org/10.4172/2090-0902.1000240

36. H. N. Hassan, H. K. Saleh, Fourier Spectral Methods for Solving Some Nonlinear Partial Differential Equations, *Int. J. Open Problems Compt. Math*, **6** (2013), 2. https://doi.org/10.12816/0006177

37. B. Karakoc, T. Ak, Numerical Simulation of Dispersive Shallow Water Waves with Rosenau-KdV Equation, *Int. J. Adv. Appl. Math. Mech.*, **3** (2016), 32–40.

38. X. Wang, W. Dai, A Conservative Fourth-Order Stable Finite Difference Scheme for the Generalized Rosenau–KdV Equation in Both 1D and 2D, *J. Comput. Appl. Math.*, **355** (2019), 310–331. http://doi.org/10.1016/j.cam.2019.01.041

39. B. Wongsaijai, K. Poochinapan, A Three-Level Average Implicit Finite Difference Scheme to Solve Equation Obtained by Coupling the Rosenau–KdV Equation and the Rosenau–RLW Equation, *Appl. Math. Comput.*, **245** (2014), 289–304. http://doi.org/10.1016/j.amc.2014.07.075

AIMS Press